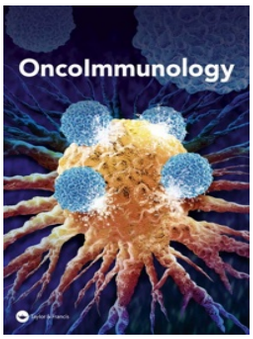

OncoImmunology

ISSN: 2162-402X (Online) Journal homepage: www.tandfonline.com/journals/koni20

Monocytes acquire a tumor-associated IL1B program upon encountering patient-derived colon cancer organoids

Bianca M. Balzasch, Andreas von Kries, Saskia Hüll , Indra A. Shaltiel, Kim E. Boonekamp, Volker Ast , Elke Burgermeister, Johannes Betge, Matthias Ebert , Michael Boutros , Laura Helming, Viktor Umansky & Adelheid Cerwenka

To cite this article: Bianca M. Balzasch, Andreas von Kries, Saskia Hüll , Indra A. Shaltiel, Kim E. Boonekamp, Volker Ast , Elke Burgermeister, Johannes Betge, Matthias Ebert , Michael Boutros , Laura Helming, Viktor Umansky & Adelheid Cerwenka (2026) Monocytes acquire a tumor-associated IL1B program upon encountering patient-derived colon cancer organoids, OncoImmunology, 15:1, 2633012, DOI: 10.1080/2162402X.2026.2633012

To link to this article: https://doi.org/10.1080/2162402X.2026.2633012

ONCOIMMUNOLOGY
2026, VOL. 15, NO. 1, 2633012
https://doi.org/10.1080/2162402X.2026.2633012

Taylor & Francis
Taylor & Francis Group

RESEARCH ARTICLE

Monocytes acquire a tumor-associated IL1B program upon encountering patient-derived colon cancer organoids

Bianca M. Balzasch[a], Andreas von Kries[a], Saskia Hüll[a], Indra A. Shaltiel[a], Kim E. Boonekamp[b,c], Volker Ast[d], Elke Burgermeister[e], Johannes Betge[e,f,g,h], Matthias Ebert[e,f,h,i], Michael Boutros[b,c], Laura Helming[j], Viktor Umansky[f,k,l] and Adelheid Cerwenka[a,f,m]

[a]Department of Immunobiochemistry, Mannheim Institute for Innate Immunoscience (MI3), Medical Faculty Mannheim, Heidelberg University, Mannheim, Germany; [b]German Cancer Research Center (DKFZ), Division Signaling and Functional Genomics, Heidelberg, Germany; [c]Medical Faculty Heidelberg, Institute for Human Genetics, Heidelberg University, Heidelberg, Germany; [d]NGS Core Facility Mannheim, Medical Faculty Mannheim, University of Heidelberg, Mannheim, Germany; [e]Department of Medicine II, Medical Faculty Mannheim, Heidelberg University, Mannheim, Germany; [f]DKFZ-Hector Cancer Institute at the University Medical Center, Mannheim, Germany; [g]Junior Clinical Cooperation Unit Translational Gastrointestinal Oncology and Preclinical Models, German Cancer Research Center (DKFZ), Heidelberg, Germany; [h]Mannheim Cancer Center (MCC), Medical Faculty Mannheim, Heidelberg University, Mannheim, Germany; [i]Molecular Medicine Partnership Unit, European Molecular Biology Laboratory, Heidelberg, Germany; [j]Research Unit Oncology, EMD Serono, EMD Serono Research & Development Institute, Billerica, MA, USA; [k]German Cancer Research Center (DKFZ), Skin Cancer Unit, Heidelberg, Germany; [l]Department of Dermatology Venereology and Allergology, University Medical Centre Mannheim, Heidelberg University, Mannheim, Germany; [m]European Center for Angioscience (ECAS), Medical Faculty Mannheim, Heidelberg University, Mannheim, Germany

ABSTRACT

Tumor-associated macrophages (TAMs) and monocytes that accumulate in colorectal cancer (CRC) play a crucial role in shaping the tumor microenvironment (TME) and anti-tumor immune responses. Although TAMs have been linked to both pro- and anti-tumor functions, our understanding of the cues instructing their heterogeneous phenotypes and function in cancer patients remains limited. Here, we established co-cultures comprising primary human monocytes and patient-derived organoids (PDOs) from patients with microsatellite-stable CRC to emulate myeloid/tumor cell interactions *in vitro*. Upon encountering PDOs, monocytes acquire phenotypic changes that are distinct from those induced by typical polarization protocols. Single-cell RNA sequencing revealed that PDO-exposed monocytes transcriptionally resembled IL1B-programmed monocytes previously identified in the tumor tissues of CRC patients. This phenotype emerged independently of tumor mutational profiles or consensus molecular subtypes. Mechanistically, soluble PDO-derived mediators induced the production of CXCL2, CXCL5 and CXCL7 chemokines, whereas the phagocytic uptake of tumor debris impaired the MHC class II-mediated antigen presentation capabilities of monocytes in co-culture. In addition, our *in vitro* system allowed functional assessment of PDO-exposed monocytes demonstrating a compromised capacity to mount an inflammatory response upon TLR stimulation. Together, PDO–monocyte co-cultures offer a platform to dissect the interplay between cancer cells and monocytes, and advance our understanding of myeloid plasticity and function in cancer patients.

ARTICLE HISTORY
Received 2 December 2025
Revised 4 February 2026
Accepted 12 February 2026

KEYWORDS
Organoid; tumor-associated macrophages; IL1B; colon cancer

Introduction

Colorectal cancer (CRC) is one of the leading causes of cancer-related morbidity and mortality worldwide, and is characterized by substantial molecular heterogeneity. In addition to malignant cells, the tumor microenvironment (TME) plays a pivotal role in disease progression, therapy response, and immune evasion. Four consensus molecular subtypes (CMS1-4) stratify CRC patients into groups with distinct biology, reflecting not only the genetic, epigenetic and metabolic status but also stromal and immune infiltration within the TME.[1] Among the immune components of the TME, myeloid cells—particularly

CONTACT Adelheid Cerwenka adelheid.cerwenka@medma.uni-heidelberg.de Mannheim Institute for Innate Immunoscience (MI3), Heidelberg University, Medical Faculty Mannheim, TPMA2 Franz-Volhard Str. 6, 68167, Mannheim, Germany
Supplemental data for this article can be accessed online at https://doi.org/10.1080/2162402X.2026.2633012.

tumor-associated macrophages (TAMs) and monocytes—have emerged as central players orchestrating immune cell organization and function in CRC.[2] Although TAMs are often associated with tumor progression, angiogenesis, immunosuppression, and resistance to therapy, their impact on CRC appears to be context-dependent, with considerable patient-to-patient variability.[3,4]

TAMs are shaped by multiple factors including their ontogeny, local signals encountered in the TME, and their potential to establish and maintain tissue residency.[5] While tissue-resident macrophages derived from embryonic progenitors sense the early events of malignant transformation, circulating monocytes recruited to the TME are the predominant source of TAMs in CRC.[6] Single-cell RNA sequencing of human CRC has revealed remarkable heterogeneity within the myeloid compartment, reflecting the plasticity of these cells in response to various environmental cues.[2,7,8] Recent efforts to harmonize the nomenclature by compiling atlases such as the MoMacVerse compendium have helped to capture TAM diversity across organs and diseases in a unified framework.[9] However, our understanding of the formation, function, and therapeutic potential of human TAM subsets and their potential to respond to TME-derived factors in individual patients remains limited. Moreover, species-specific differences in TAM biology hamper transferability of findings from clinically relevant mouse models to the human setting.[10]

Patient-derived organoids (PDO) have provided critical insights into tumor cell-intrinsic biology by depicting not only the genetic and epigenetic profiles of individual patients, but also retaining the tissue architecture observed *in vivo*.[11] However, PDOs inherently lack immune and stromal compartments, thereby hindering the investigation of cell-cell interactions that underlie inflammation and immune modulation. More recently, next-generation PDO models have incorporated immune cells, enabling the study of how epithelial tumors shape the immune compartment.[12] Current PDO models studying TAM-cancer cell interactions utilize *in vitro* differentiated macrophages as a source of the myeloid compartment,[13-15] offering insights into human TAM biology, but not into the differentiation processes of circulating monocytes as they encounter the tumor tissue. This process is of major importance in CRC, where the majority of infiltrating TAMs are recruited from the circulation.[6]

Here, we present a primary monocyte-PDO co-culture model to investigate how human CRC cells instruct monocyte differentiation and activation. Across a range of PDOs derived from individual patients with microsatellite-stable CRC, monocytes consistently acquired a broadly shared phenotype in co-culture, irrespective of the mutational background of the individual tumor. Single-cell RNA sequencing revealed that this program resembled the molecular features of a subset of monocytes observed in CRC tumors referred to as IL1B monocytes. In fact, PDOs effectively shaped both the pro-inflammatory and pro-tumoral features of IL1B monocytes. Together, our data revealed that contact with the CRC epithelium is sufficient to instruct the differentiation of IL1B-programmed monocytes, and provide a tractable system to interrogate monocyte function in CRC.

Materials and methods

Patient cohort

Biopsies were obtained from eight primary tumors of treatment-naïve patients with microsatellite-stable CRC with a new diagnosis of colorectal cancer by endoscopy as part of the clinical diagnostics at the University Medical Center Mannheim, Heidelberg University. The samples of the cohort were collected during the year 2017–2022, and patients with active HIV, HBV and HCV infection were excluded. Clinical data and tumor characteristics are mentioned in Supplemental Table S1. Written informed consent was obtained from all study participants prior to sample collection, and material collection complied with all relevant institutional/governmental regulations.

PDO culture

CRC PDOs were generated and cultured in basement membrane extract BME (R&D Systems) as described previously.[16] The PDO culture medium (ENA) was composed of ENA_{basal} (Advanced DMEM/F12 (Gibco) medium with Pen/Strep (Gibco), Glutamax (Gibco) and HEPES (Gibco)) supplemented with 100 ng/ml noggin (Peprotech), 1X B27 (Gibco), 1.25 mM *n*-acetyl-cysteine (Sigma-Aldrich), 10 mM nicotinamide

(Sigma-Aldrich), 50 ng/ml human EGF (Sigma-Aldrich), 10 nM Gastrin (Peprotech), 500 nM A83-01 (Sigma-Aldrich), 10 nM Prostaglandin E2 (Biomol), 10 µM Y-27632 (Biomol) and 100 mg/ml Primocin (Invivogen). After 4–5 d of culture, the medium was replaced with ENA medium lacking the apoptosis inhibitor Y-27632. After 7–8 d, the PDOs were washed with PBS, digested with TrypLE Express Enzyme (Thermo Scientific) at 37 °C to obtain single-cell solutions, counted, and re-seeded.

Human primary monocyte isolation

Peripheral blood mononuclear cells (PBMCs) of healthy blood donors were isolated by gradient centrifugation using Pancoll (PAN Biotech). Ethical approval and written patient consent were obtained from all blood donors. $CD14^+$ monocytes were subsequently isolated by negative selection using the EasySep Human Monocyte Isolation Kit (StemCell), according to the manufacturer's protocol.

PDO/Monocyte co-cultures

PDOs cultured for 5–7 d were retrieved by washing with PBS, and incubated twice in CellRecovery solution (Corning) for 10 min on ice. The BME-free PDOs were resuspended in PBS and kept on ice until seeding. An aliquot of the PDO suspension was counted after single-cell digestion as described previously.

For the PDO/monocyte co-cultures, freshly isolated monocytes and PDOs were resuspended in co-culture medium containing 20 ng/ml M-CSF and liquid 5% BME at a ratio of 2:1 (immune cell: PDO cell). The co-culture medium was freshly prepared by mixing equal parts of monocyte medium (RPMI-1640 (Sigma-Aldrich) supplemented with 10% heat-inactivated FCS (Sigma-Aldrich), 100 U/ml Pen/Strep (Gibco), 1 mM Sodium Pyruvate (Gibco), 1X NEAA (Gibco), 55 µM β-mercaptoethanol (Sigma-Aldrich), and ENA medium, excluding the apoptosis inhibitor Y-27632 and nicotinamide. Monocyte/PDO were co-cultured as suspension cultures in UpCell culture plates (Thermo Scientific) for 2–4 d at 37 °C.

During co-culture experiments using small molecule inhibitors, monocytes were pretreated with 2 µM BAY11-7082 (InvivoGen), 10 µM Cytochalasin D (Sigma-Aldrich), or DMSO vehicle control (<0.2%) for 30 min prior to addition of PDOs. Inhibitors were present throughout co-culture.

Conditioned PDO medium was generated by seeding PDOs in suspension monoculture at the same cell concentration as the co-cultures. After 4 d, the medium was harvested by centrifugation twice at 2000 rpm for 10 min, passed through a 0.22 µm filter and frozen as aliquots at –80 °C for further use. Conditioned PDO medium was mixed in equal parts with fresh co-culture medium.

For TLR stimulation, PDO/monocyte co-cultures were stimulated after four days with 100 ng/ml LPS (Sigma) or 1000 ng/ml Pam3CSK4 (InvivoGen) in the presence of the protein transport inhibitor GolgiPlug (BD Biosciences). After 5 h of stimulation, the cells were analyzed using flow cytometry.

Chemokine quantification

Cell culture supernatants were collected and centrifuged twice at 2000 rpm for 10 min before storage at –80 °C. Chemokines were quantified using DuoSet ELISA kits (R&D Systems) according to the manufacturer's instructions. The absorbance was recorded at 450 nm (reference: 540 nm) using a Spark Multimode microplate reader (Tecan).

Flow cytometry

Cells were harvested, passed through a 40 µm filter to remove PDOs, and washed with PBS. For flow cytometry analysis, monocytes were stained with the ZombieAqua Fixable Viability Kit (BioLegend) for 10 min, followed by another 10 min of treatment with FcR blocking TrueStain (BioLegend). Subsequently, the cells were stained with the following monoclonal fluorochrome-conjugated antibodies for 30 min at 4 °C: CD14-FITC (clone HCD14), CD16-BV785 (clone 3G8), CD39-APC (clone A1), CD40-BV605 (clone 5C3), CD45-FITC (clone HI30), CD73-BV711 (clone AD2), CD86-PE (clone BU63), CD163-BV785 (clone GHI/61), CD206-BV605 (clone 15-2), CXCR4-PE-Cy7 (clone 12G5), CX3CR1-PE (clone 2A9-1), EpCAM-APC (clone 9C4), HLA-DR-APC-Cy7

(clone L243), PD-L1-PE (clone MIH2), TIM4-APC (clone 9F4). Further information on the supplier and RRID are listed in Supplemental Table S2. Cells were washed and analyzed on LSRFortessa X-20 (BD Bioscience, RRID:SCR_025285). For FACS sorting, the cells were stained with 7-AAD (BD Bioscience), washed with PBS and diluted in PBS/EDTA (2 mM) to a concentration of $1–2 \times 10^6$ cells/mL. Cell sorting was performed using the FACS ARIA Fusion (BD Bioscience, RRID:SCR_025715).

For intracellular staining, cells were fixed and permeabilized with CytoFix/CytoPerm Fixation/Permeabilization kit (BD Bioscience) according to the manufacturer's instructions, and stained with TNF-α-APC (clone Mab11, BioLegend) for 30 min at 4 °C (see Supplemental Table S2). After one wash, cells were analyzed on the LSRFortessa X-20.

For the detection of phosphoproteins, cells were fixed at 37 °C with warm Cytofix fixation buffer (BD Biosciences) for 10 min, spun down, and resuspended in ice-cold Phosflow Perm Buffer III (BD Biosciences). Cells were incubated on ice for 30 min prior to staining with fluorochrome-conjugated antibodies CD45-FITC (clone HI30) and NF-κB p65-PE (pS529, clone K10-895.12.50) (see Supplemental Table S2). Acquisition was performed using the LSRFortessa X-20.

Flow cytometry data were analyzed with FlowJo V.10.9.0 (BD Bioscience).

Live-cell imaging

To quantify PDO growth, co-cultures were seeded in flat-bottom 96-well cell culture plates (4–6 technical replicates per condition) and placed in an SX5 IncuCyte system (Sartorius, RRID:SCR_026298). Brightfield images of the PDO monoculture and co-cultures were acquired every 4 h (10x objective, multi-spheroid mode) and analyzed using the SX5 IncuCyte software. PDOs were segmented and quantified using brightfield images (μm^2/Image). To assess the PDO growth, the initial total area measured at time point 0 was subtracted from each subsequent measurement.

For live confocal fluorescence light microscopy, co-cultures with CellTrace far-red (ThermoFisher)-stained monocytes were seeded in ibiTreat 8-well polymer μ-Slides (Ibidi) in the presence of 0.5 µg/mL CellMask Orange membrane dye (ThermoFisher). Images were acquired every 10 min on a LSM800 confocal microscope (Zeiss, RRID:SCR_015963) with a 20×(0.8) objective exciting sequentially with 561-nm and 640-nm laser lines and analyzed in ImageJ.

Cell viability assay

Cell viability of monocultures and co-cultures was determined using the CellTiter-Glo3D cell viability assay (Promega) according to the manufacturer's instructions. Luminescence was recorded using a Spark Multimode microplate reader (Tecan, RRID:SCR_021897).

Generation of iRFP-PDO line

A lentiviral expression vector for membrane localization of miRFP680 was generated by cloning miRFP680 from pmiRFP680-N1 (Addgene, RRID: Addgene_136557) into a lentiviral backbone (pLenti6.2_mTagBFP2, Addgene, RRID: Addgene_113725) together with a membrane localization signal, the *N*-terminal 20 amino acids of neuromodulin, also called GAP-43 (source: light microscopy facility DKFZ). pLenti-Mem-miRFP680 was packaged into lentiviral particles and transduced into the PDO line PDO7. Cells expressing the constructs were sorted by flow cytometry.

Single-cell sequencing and analysis of monocytes

Cell preparation and data generation

Monocyte monoculture (M_d4) and co-cultures with either PDO19 (M_PDO19) or PDO30 (M_PDO30) were prepared using monocytes from three different donors, as described above. Polarized monocytes were prepared for each donor by treating for 24 h prior to harvesting with 100 ng/ml LPS + 100 ng/ml IFN-g (M_LPS/IFNg) or 20 ng/ml IL-4 (M_IL4). After 4 d of culture, cells were harvested by filtering through a 40 µm strainer, followed by counting and pooling cells derived from the three different donors. Live $CD45^+$

cells were sorted by flow cytometry as described above. Additionally, monocytes of each of the three donors were prepared 16 h after immune cell isolation (M_d0) to provide an undifferentiated control.

The sorted single-cell suspensions were loaded onto a Chromium Single-Cell Controller (10X Genomics) for droplet-based single-cell capture, according to the manufacturer's protocol. Subsequent library preparation was performed according to the Chromium Next GEM Single Cell 3' GEM, Library & Gel Bead Kit v3.1 (10X Genomics, 14–16 cycles). Quality and quantity of the libraries were evaluated using a Bioanalyzer (Agilent) and Qubit (ThermoFisher), respectively. Sequencing was performed on an Illumina NovaSeq 6000 platform (paired-end, 150 bp reads length).

Data processing and quality control

Single-cell sequencing data were processed with 10x Genomics Cell Ranger v7.0.0 software using the human reference genome GRCh38-3.0.0. Each pooled sample was subsequently demultiplexed using the SNP-based demultiplexing tool Freemuxlet.[17] Briefly, we used the high-confidence SNP data from 1000 genomes project (hg38_v0_1000G_phase1.snps.high_confidence.hg38.vcf) as a reference. The SNP file was filtered and sorted according to the chromosomal order in the respective bam files. The bam files were also sorted by chromosomal positions and filtered using the poscle helper script filter_bam_file_for _popscle_dsc_pileup.sh to keep only reads which are covered by SNPs. The tool dsc-pileup was then used to build pileups from aligned sequence reads around known SNPs for each pooled sample. Finally, freemuxlet was utilized to identify single samples from the pileup files. Barcodes were assigned to single samples by filtering the feemuxlet output for singlets (DROPLET.TYPE == "SNG") and samples IDs (BEST.GUESS == "0, 0" for sample 1 etc.).

Gene counts and donor IDs were imported into R (v4.3.2) and processed with Seurat (v5.2.1).[18] For quality control, genes detected in less than three cells and cells flagged as doublets by feemuxlet were removed. Moreover, cells with a unique feature count of less than 200 and with more than 25% of mitochondrial gene counts were excluded. The upper limits of feature counts were set to 6000 for each data set. The filtered raw expression data of all samples were merged and normalized via the SCTransform function of the Seurat v5 pipeline, regressing out the mitochondrial percentage. After principal component analysis, samples were integrated using Harmony[19] to correct for the donor ID as batch effect, implemented by the RunHarmony function. 91 cells showed a T cell expression pattern and were therefore excluded from further analysis.

Clustering and data visualization

The first 40 harmony dimensions were used to compute the shared nearest neighbor (SNN) graph using the FindNeighbors function. Clusters were identified using the FindClusters function (resolution 0.8) and visualized by UMAP.

Differential gene expression (DEG) analysis

DEG with respect to culture conditions were identified by the FindAllMarkers function of the Seurat v5 pipeline applying the MAST algorithm[20] with the following criteria: only.pos = FALSE and min.pct = 0.2. Venn diagrams were created using the VennDiagram package (v1.7.3) and heatmaps were created using the ComplexHeatmap package (v2.18.0).[21]

Pathway and module enrichment analysis

The clusterProfiler package (v4.10.1)[22] was applied to conduct gene set enrichment analysis (GSEA) using the Gene Ontology and Hallmark databases with org.Hs.eg.db (v3.18.0) annotation. Gene signatures related to M1/M2 macrophages or MoMacVerse subsets (see Supplemental Table S3) were evaluated using the UCell package (v2.6.2)[23] applying the AddModuleScore_UCell function. Pathway and transcription factor activity inference were performed using PROGENy (v1.11.3) and DoRothEA (v1.14.1) packages, respectively.[24,25]

Cell label transfer from the MoMacVerse

The MoMacVerse[9] provided as RDS file by Gustave Roussy FG-Lab Resources was processed with Seurat. First, the atlas was reduced to cells of CRC patients, and non-relevant cells were removed including

"proliferating cells -10", "Tcell Doublets -9" and "DC2/3 -14". Next, a reference UMAP was generated by setting return.model = TRUE and running RunUMAP. Finally, cell label transfer to our query dataset was performed using FindTransferAnchors and MapQuery functions from Seurat.

Bulk sequencing and analysis of PDO cells

PDO30 from four days of mono- or co-culture were dissociated to single cells and prepared for FACS, as described previously. Live $EpCAM^+$ cells were sorted into chilled RLT lysis buffer. RNA was isolated using the RNeasy Mini Kit (Qiagen) according to the manufacturer's instructions. RNA libraries were prepared by enriching mRNA using the NEBNext Poly(A) mRNA Magnetic Isolation Module (New England BioLabs) followed by the NEBNext Ultra II Directional RNA Library Prep Kit (New England BioLabs), according to the manufacturer's instructions. Quality and quantity of the libraries was evaluated using a Bioanalyzer (Agilent) and Qubit (ThermoFisher), respectively. The libraries were sequenced on a llumina NovaSeq 6000 platform (paired end, 150 bp read length). Bulk RNA-seq data were analyzed as previously described.[26]

Statistical analysis

Statistical analyzes were performed using either GraphPad Prism v10.2.3 (GraphPad Software) or R studio v3.4.2 (R Project). Differences were considered statistically significant at a p-value of < 0.05 and depicted as *, $p < 0.05$; **, $p < 0.005$; ***, $p < 0.001$; and ****, $p < 0.0001$. Data were tested for normal distribution using the Shapiro-Wilk test and subsequently evaluated using the test indicated in the Figure legends. Correction for multiple comparisons was performed when necessary. Data are presented as mean ± standard deviation.

Results

Colon cancer PDOs induce phenotypic changes in primary peripheral blood human monocytes regardless of tumors' mutational profile

To investigate the interaction of monocytes encountering a patient-specific CRC TME, we developed a co-culture system comprising primary human monocytes from buffy coats of healthy donors and PDOs generated from biopsies from microsatellite-stable CRC. We employed a recently described panel of eight PDOs[16] derived from patients across AJCC/UICC stages and two CMS subtypes (CMS2/CMS3), reflecting the heterogeneous mutational spectrum of microsatellite-stable CRC, including key driver mutations in *APC*, *KRAS* and *TP53* (Figure 1A and B, Supplemental Table S1). To support monocyte viability and recovery while not affecting PDO growth, we optimized the co-culture medium composition and applied a low-viscosity extracellular matrix (Figures 1C and S1). Under these experimental conditions, PDOs increased consistently in size over time regardless of the presence or absence of monocytes, indicating neither growth-inhibiting nor growth-promoting function of monocytes on CRC PDOs (Figure 1D). Monocytes did not infiltrate the PDO 3D structures, in agreement with a previous study that utilized PBMCs in PDO co-cultures.[27]

To determine phenotypic changes when exposed to individual PDOs, we analyzed monocytes derived from PDO co-cultures or from four days in monocultures based on the expression of surface proteins associated with monocyte classification, tissue homing, and activation as well as with an immunosuppressive myeloid phenotype (Figure 1E and F). Upon interaction with PDOs, monocytes acquired the expression of proteins associated with colon tissue residency such as CX_3CR_1 and TIM4,[28] alongside the upregulation of CXCR4 and CD73, proteins linked to tissue homing of myeloid subsets with pro-angiogenic and immunosuppressive functions, respectively.[29,30] The expression of the canonical monocyte subset markers CD14 and CD16 remained similar on cells cultured in the presence or absence of PDOs. In contrast, the expression of CD206, which is frequently observed on TAMs, was reduced on monocytes derived from PDO co-culture compared to monoculture, together with key proteins involved in T cell stimulation, including HLA-DR, CD40 and CD86. The expression of another archetypical TAM marker,

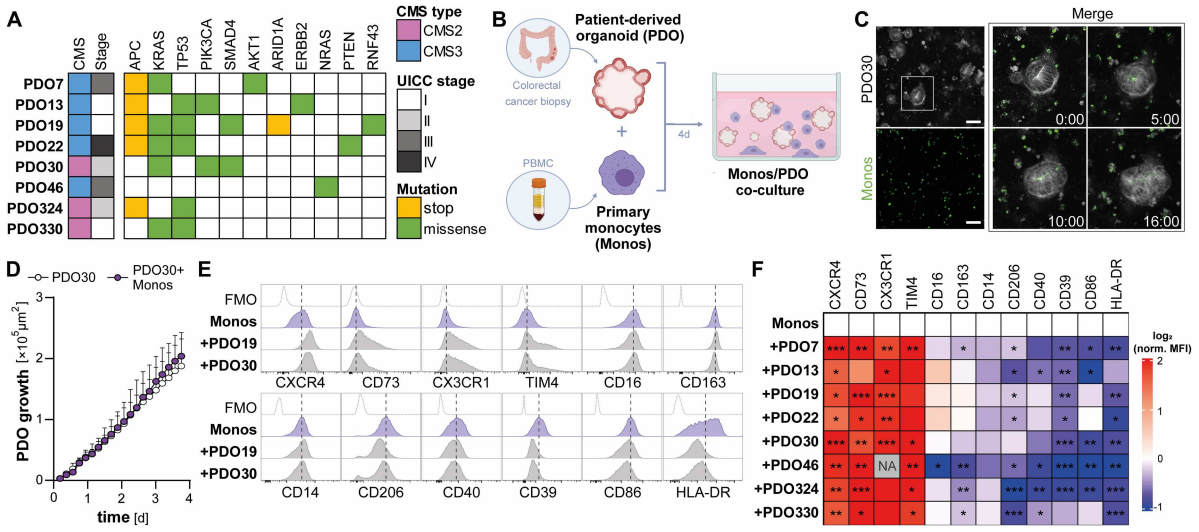

Figure 1. PDOs induce similar monocyte phenotypes in co-culture. (A) Characteristics of PDOs including consensus molecular subtypes (CMS), AJCC/UICC stage and mutation status. (B) Experimental set-up of primary monocyte/PDO co-culture in 5% BME suspension matrix. (C) Representative live-cell images of monocytes in co-culture with PDO30 over time. Monocytes were labeled with CellTrace Far Red prior to co-culture and plasma membranes stained with CellMask Orange (time in hours, scale bar: 100 µm). (D) Growth of PDO30 in monoculture or co-culture (immune cell to PDO cell ratio at the start of the culture 2:1) monitored by live-cell imaging using the IncuCyte SX5. Mean+SD, $N = 4$ monocyte donors with 4–6 technical replicates. (E,F) Surface protein expression on live CD45$^+$ monocytes in monoculture or co-culture with PDO lines measured by flow cytometry after four days. Representative histograms for monocytes in mono- and co-cultures with PDO19 and PDO30 in (E), and quantification of the expression relative to monocyte monoculture in (F). The MFI was normalized to respective monocyte donor in monoculture and log2 transformed, asterisks inside the heatmap indicate significance according to results of One-Way ANOVA. Mean, $N = 8–14$ monocyte donors, $^*p < 0.05$,$^{**}p < 0.01$, $^{***}p < 0.001$, FMO = fluorescence minus one, NA = not assessed.

CD163, on PDO-exposed monocytes was more variable and depended on the PDO studied. Notably, PD-L1 was not detected on PDO-co-cultured monocytes (data not shown). While we observed variability in the monocyte phenotype in co-culture, the overall patterns of phenotypic changes of monocytes were consistent across PDO co-cultures and monocyte donors.

Taken together, primary human monocytes undergo phenotypic changes extending beyond classical TAM markers such as CD163 and CD206 upon interaction with PDOs derived from individual CRC patients, irrespective of their mutational profiles.

PDOs evoke distinct transcriptional states in monocytes

To obtain further insight into PDO-induced changes of the myeloid cell state, single-cell RNA sequencing (scRNA-seq) of monocytes derived from PDO co-culture and monoculture was performed (Figure 2A). For this study, we selected PDO19 and PDO30 as representatives of the CRC CMS2 and CMS3 subtypes. Monocytes isolated after a four-day co-culture with PDO19 or PDO30 were termed M_PDO19 and M_PDO30, respectively. In parallel, monocytes directly after isolation from buffy coats (M_d0), four days after monoculture (M_d4), pro-inflammatory monocytes induced by LPS/IFN-γ treatment (M_LPS/IFNg) or IL-4 stimulated anti-inflammatory monocytes (M_IL4)—as reference polarization states described in the literature[31]—were subjected to scRNA-seq. The final dataset comprised 17 822 single cells passing quality control (>200 detected genes and <25% mitochondrial gene content per cell, >90% of sequenced cells), with balanced representation of the three tested monocyte donors (Figure S2).

Monocytes derived from either PDO19 or PDO30 co-culture mapped into an overlapping uniform manifold approximation and projection (UMAP) space that was distinct from monocytes M_d0 and M_d4 without PDO contact, as well as from polarized pro-inflammatory and anti-inflammatory monocytes (Figure 2B). Moreover, gene signatures classifying macrophages into M1 or M2,[32,33] which are commonly utilized to stratify TAMs in patients, were not enriched in PDO-programmed monocytes (Figure 2C).

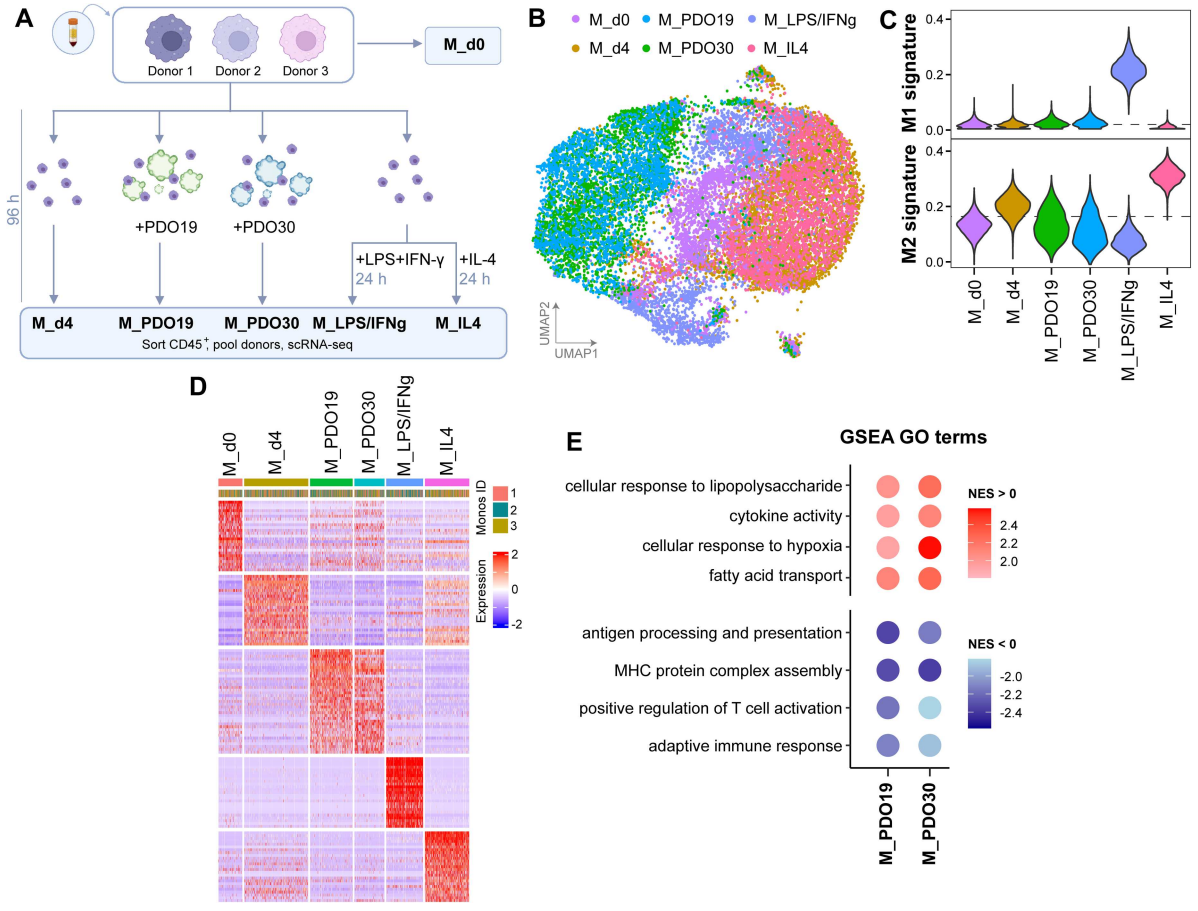

Figure 2. PDO co-culture induces distinct transcriptional state in monocytes. (A) Experimental design of scRNA-seq experiment: FACS-sorted live CD45^{+} monocytes were sequenced after 96 h of PDO co-culture with PDO19 (M_PDO19) or PDO30 (M_PDO30). Additionally, monocytes were sorted and sequenced directly after isolation from buffy coats (M_d0), after 96 h of culture (M_d4), or treatment with LPS+IFN-γ (M_LPS/IFNγ) or IL-4 (M_IL4) for the final 24 h. $N = 3$ monocyte donors. (B) Uniform manifold approximation and projection (UMAP) representation of scRNA-seq data. (C) Violin plots depicting enrichment scores of common M1 and M2 signature genes described by Azizi *et al.* (2018), on scRNA-seq data set comprising monocytes stratified by culture condition described in (A). The dashed line denotes the median score of the complete dataset. (D) Heatmap of top 50 differentially expressed genes (DEGs) from monocytes of each culture condition described in (A). (E) Dot plot of top pathways (GO biological processes) enriched or downregulated in PDO-exposed monocytes compared to other culture conditions by gene set enrichment analysis (GSEA) (normalized enrichment score NES > 2 | NES < −2).

Calculating differentially expressed genes (DEGs) comparing monocytes of all experimental conditions (DEGs expressed in 20% of cells, FC > 1, adj.p.val < 0.05) highlighted the acquisition of a distinct transcriptomic state in PDO-programmed monocytes that was similar between monocytes derived from PDO19 or PDO30 co-cultures (Figure 2D). Pathway analysis revealed that the interaction with either PDO enriched a shared transcriptional response related to inflammation, hypoxia, and lipid metabolism compared to all other sequenced monocytes (Figure 2E). Consistent with the results of our initial immune cell phenotyping (Figure 1), expression of genes involved in Gene Ontology (GO) terms linked to antigen presentation and processing and regulation of T cells were reduced in M_PDO19 and M_PDO30 cells.

In summary, single-cell transcriptome analysis revealed a common monocyte programming following the interaction with both tested PDOs that extended beyond the traditional M1/M2 dichotomy. This suggests that upon encountering the tumor tissue, monocytes adopt a transcriptional state characterized by the concurrent expression of genes associated with inflammatory signaling and pro-tumor features, including a limited antigen presentation capacity, and activation of hypoxic and pro-angiogenic pathways.

Monocytes in PDO co-culture acquire a program related to the phenotype of tumor-associated IL1B monocytes identified in CRC patients

Next, we aimed to contextualize monocytes generated in the PDO system within the spectrum of heterogeneous tumor-associated monocytes and macrophages described in cancer patients. The MoMacVerse provides a landmark scRNA-seq reference for human myeloid cells in cancer and other diseases, designed to support harmonized annotation and comparison of myeloid phenotypes across different tissues.[9] We curated a colon tissue-focused MoMacVerse and projected our samples into this reference space (Figure 3A and B). After label transfer of defined MoMacVerse states, PDO-exposed monocytes mapped predominantly to IL1B monocytes (MoMac cluster 15, inflammation-associated), TREM2 macrophages (MoMac cluster 3, lipid metabolism-associated), and to a lesser extent $CD16^-$ monocytes (MoMac cluster 8, classical monocytes). Monocytes differentiated for four days in mono-culture, M_d4, also fell within the MoMac cluster of TREM2 macrophages, alongside the cluster of HES1 macrophages (MoMac cluster 2, healthy colon tissue-associated), while monocytes sequenced directly after isolation (M_d0) were labeled mainly as $CD16^+$ Monocytes (MoMac cluster 5, intermediate monocytes).

To validate the mapping results, we assigned signature scores to each cell of our dataset based on the gene sets corresponding to the reported DEGs of MoMacVerse-defined states (Figure 3C). This scoring corroborated the classification of PDO-programmed monocytes as MoMacVerse IL1B monocytes, while associating TREM2 macrophages and $CD16^+$ monocytes predominantly with M_d4 cells and M_d0 cells, respectively. When examining the expression of key signature transcripts reported to define the IL1B monocyte state, M_PDO19 and M_PDO30 monocytes were enriched in multiple transcripts, encoding chemotactic molecules (*CXCL2*, *CXCL3*), growth factors linked to tissue repair and angiogenesis (*EREG*, *VEGFA*), as well as *IL1B* itself (Figure 3D). Notably, we did not detect differential IL-1β protein secretion in PDO-co-culture (data not shown).

PDOs promote NF-κB-driven chemokine production in monocytes upon co-culture

The IL1B monocyte signature enriched in M_PDO19 and M_PDO30 comprised transcripts of various chemokines, including *CXCL2* and *CXCL3*, which coincided with the observation that several chemokines were among the top 15 DEGs upregulated in monocytes after interaction with both tested PDOs (Figure 4A). To determine whether the upregulated transcripts resulted in differential chemokine production, we performed ELISA for CXCL2, CXCL5 and CXCL7 (encoded by *PPBP*) on mono- and co-culture supernatants (Figure 4B). In concordance with the transcriptomic data, we detected elevated concentrations of all tested chemokines in the supernatants of the majority of PDO–monocyte co-cultures compared to monocultured monocytes, except co-cultures with PDO13. PDOs themselves secreted negligible CXCL protein compared to monocytes, averaging an 18-fold lower secretion of CXCL2, 230-fold lower concentration of CXCL5, and less than 4000-fold secretion of CXCL7 (Figure S3A). This implied that monocytes were the dominant source of chemokines in co-culture.

To gain deeper insight into the potential signaling events underlying this pro-inflammatory activation of monocytes in PDO co-culture, we inferred the activity of well-characterized pathways based on the expression of known target and pathway genes (PROGENy[24]) (Figure 4C). NF-κB, hypoxia and TNF-α signaling were predicted as prominently activated pathways in PDO-exposed monocytes compared to M_d0 and M_d4, while other pathways like VEGF and MAPK signaling showed modest activity changes in M_PDO19 and M_PDO30. Complementary Hallmark gene set enrichment analysis further confirmed the central role of the NF-κB axis in monocytes after PDO co-culture (Figure S3B). These observations coincided with increased predicted activity of transcription factors associated with a pro-inflammatory response via the NF-κB pathway (REL, NFKB1), as inferred by regulon-based prediction of transcription factor activity (DoRothEA[25]) (Figure 4D). Of note, we also identified the induction of other pro-inflammatory (STAT3 and FOS/FOSB) and anti-inflammatory modules (SMADs) in PDO-exposed monocytes.

Given the enrichment of NF-κB related terms in our pathway analyzes of PDO-exposed monocytes and the central role of NF-κB signaling in regulating pro-inflammatory cytokine production in myeloid cells,[34] we next questioned whether NF-κB activation was required for elevated chemokine production by

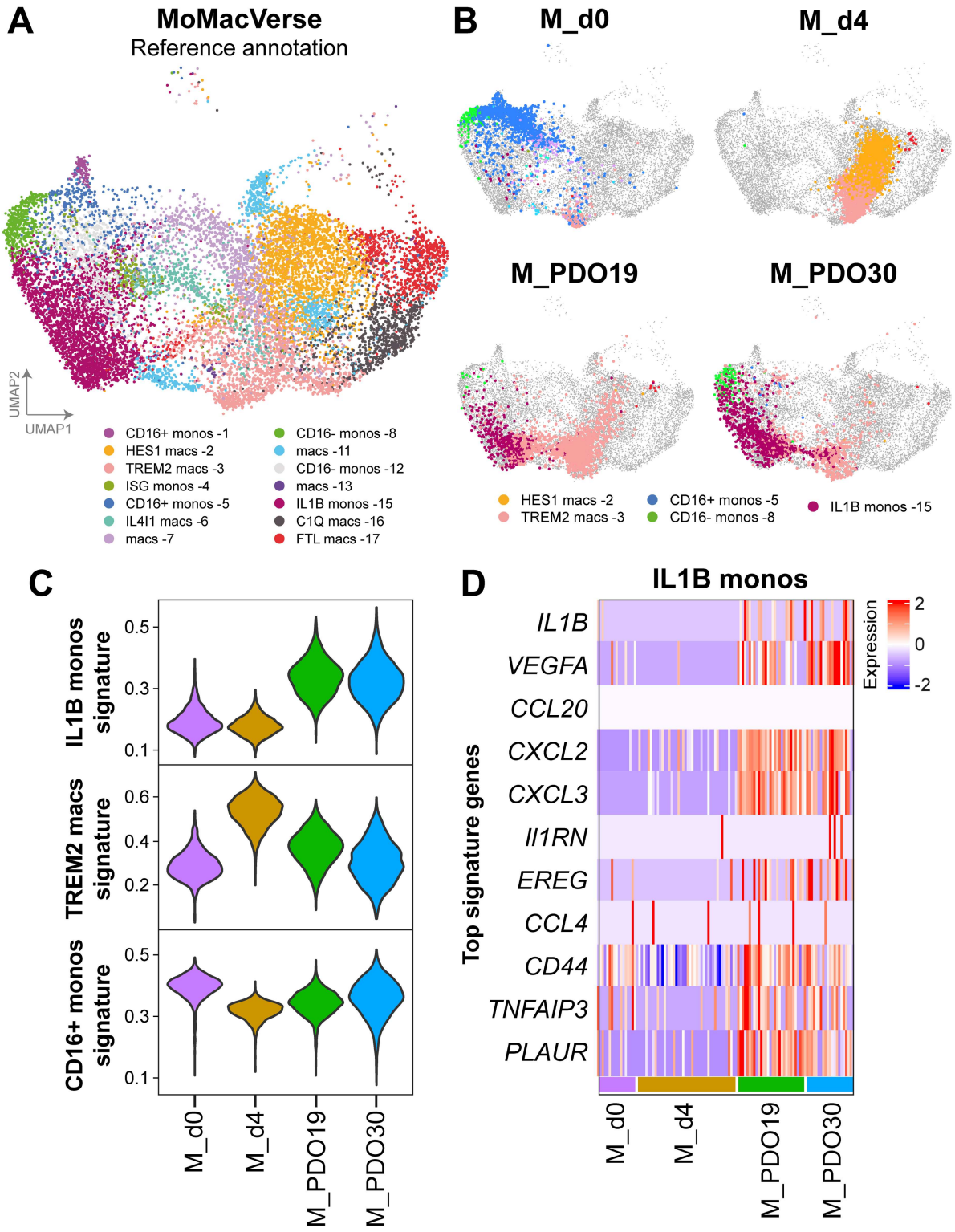

Figure 3. Monocytes in PDO co-cultures mimic an IL1B tumor-associated state identified in CRC patients. (A,B) UMAP of colon-tissue curated MoMacVerse used as query to map MoMacVerse annotations (Mulder *et al.*, 2021). Monocytes of conditions M_d0, M_d4, M_PDO19 and M_PDO30 were projected into the UMAP space of the curated MoMacVerse and annotated accordingly. (C) Violin plots depicting selected MoMacVerse signatures (UScore) expressed in monocytes derived from PDO co-cultures M_PDO19 and M_PDO30, or monocultures M_d0 and M_d4. (D) Heatmap of top IL1B monocyte signature genes as described in Mulder *et al.* (2021).

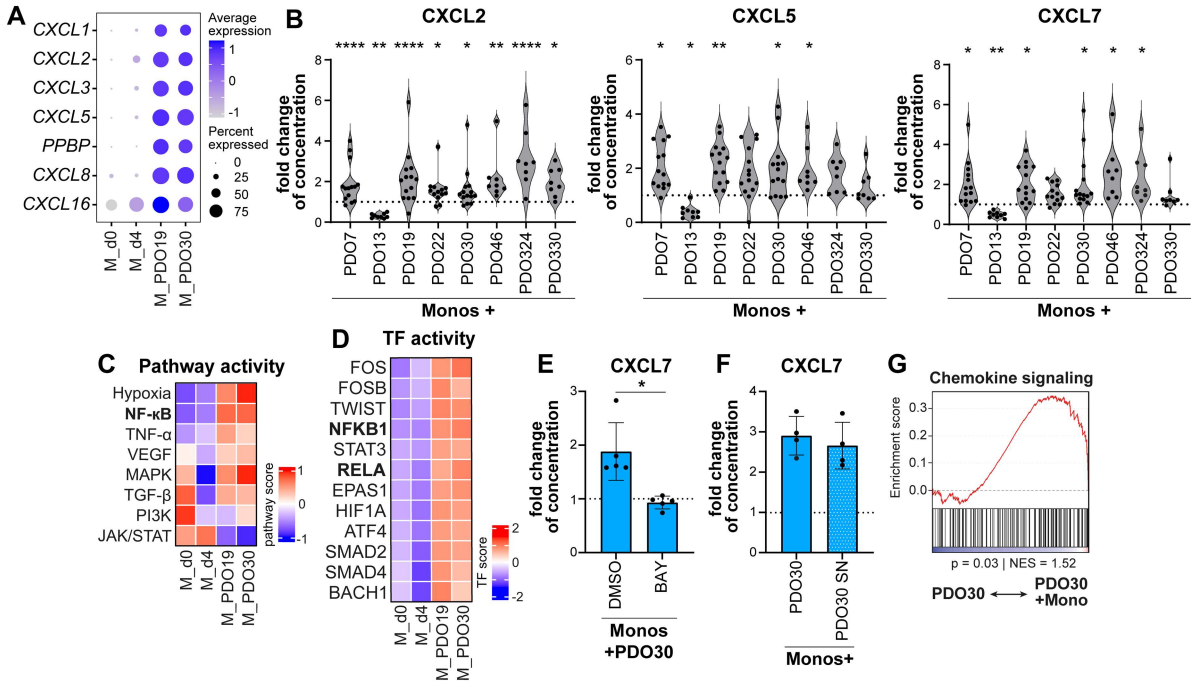

Figure 4. Chemokine secretion of monocytes in PDO co-culture is driven by NF-κB signaling. (A) Dot plot of differentially expressed chemokines in monocytes derived from PDO co-cultures or monocytes in monocultures M_d0 and M_d4. (B) Normalized CXCL2, CXCL5 and CXCL7 concentration in supernatants harvested from monocytes in co-culture with various PDO lines, as measured by ELISA. CXCL secretion in co-culture was normalized to the CXCL concentration in the supernatant of respective monocytes in monoculture, indicated by the dashed line. Mean ± SD, $N = 14–16$, One-Way ANOVA, $*p < 0.05$, $**p < 0.01$, $****p < 0.0001$. (C,D) Heatmaps depicting the pathway and transcription factor (TF) activities in monocytes after PDO co-culture or monocultures M_d0 and M_d4, inferred by PROGENy and DoRothEA analysis, respectively. (E) Normalized CXCL7 concentration in supernatants harvested from monocytes in mono- or co-culture in the presence or absence of NF-κB inhibitor BAY11-7082, as measured by ELISA. CXCL7 secretion was normalized to respective monoculture indicated by the dashed line. Mean ± SD, $N = 5$, paired t-test, $*p < 0.05$. (F) Normalized CXCL7 concentration in supernatants harvested from monocytes in co-culture with PDO30, or monocytes treated with supernatant from PDO30 monoculture (SN). CXCL7 secretion was normalized to monocyte monoculture indicated by the dashed line. Mean ± SD, $N = 4$. (G) Gene set enrichment analysis of the chemokine signaling pathway in EpCAM$^+$ sorted PDO cells comparing PDO30 exposed to monocytes with PDO30 monoculture. $N = 3$.

monocytes in PDO co-culture. Indeed, inhibition of NF-κB signaling using BAY11-7082 impaired CXCL7 secretion in co-culture (Figures 4E and S3C). To determine the role of soluble PDO-derived factors in driving myeloid NF-κB activation and chemokine production, monocytes were exposed to conditioned supernatant from PDO30 monocultures. CXCL7 production by monocytes was comparable to that observed in PDO co-cultures, indicating that the soluble factors released by PDOs mediate monocyte chemokine production (Figure 4F).

As PDO-programmed monocytes produced a broad spectrum of chemokines, we asked whether PDO cells themselves respond to these chemokines. Bulk RNA sequencing of sorted PDO30 (EpCAM$^+$) after four days in monoculture or co-culture revealed an enrichment of transcripts associated with chemokine signaling in co-cultured PDOs (Figure 4G). This implied that PDOs evoked and subsequently sensed the chemokine milieu generated by PDO-programmed monocytes.

MHC class II expression on monocytes in PDO co-culture is modulated by phagocytosis

In our scRNA-seq analysis, the enrichment of inflammatory pathways in monocytes upon PDO co-culture was accompanied by the concurrent suppression of pathways involved in antigen presentation and processing (Figure 2). In concordance with the lower expression of HLA-DR at the transcript and protein levels (Figures 1 and 5A), regulon-based prediction of transcription factor activity revealed reduced activity

of CIITA, the key transcription factor regulating HLA-DR expression, alongside reduced expression of *CIITA* in M_PDO19 and M_PDO30 (Figure 5B). This implied that the repression of antigen presentation potential upon interaction with PDOs occurred at the transcriptional level. A subsequent analysis of monocytes co-cultured with PDO30 over time showed an average reduction of 75% ± 2 in HLA-DR protein expression on monocytes detectible from day two of the co-culture (Figure 5C). To define the nature of the PDO-derived signals regulating HLA-DR expression on the surface of monocytes, we treated them with conditioned supernatants from PDO30 monocultures. In contrast to the modulation of chemokine secretion, the secreted factors of PDO30 were not sufficient to reduce HLA-DR expression on monocytes to the same extent as in the presence of PDOs (Figure 5D).

Since our results pointed at a cell-cell contact-dependent mechanism modulating HLA-DR expression, we investigated whether phagocytosis, a central process by which myeloid cells scavenge their micro-environment, could be involved. To monitor the phagocytic uptake of PDO-derived particles, we generated a PDO line stably expressing a membrane-bound far-red fluorescent protein (iRFP-PDO). Over the course of a four-day co-culture with monocytes, the frequency of iRFP$^+$ monocytes progressively increased, with an average of 50% ± 5 of the population exhibiting an iRFP signal indicative of recent phagocytosis of PDOs (Figure 5E). Inhibition of phagocytosis using Cytochalasin D significantly reduced the number of iRFP$^+$ monocytes and preserved largely, but not completely, the HLA-DR expression on monocytes in PDO co-culture (Figure 5F and G).

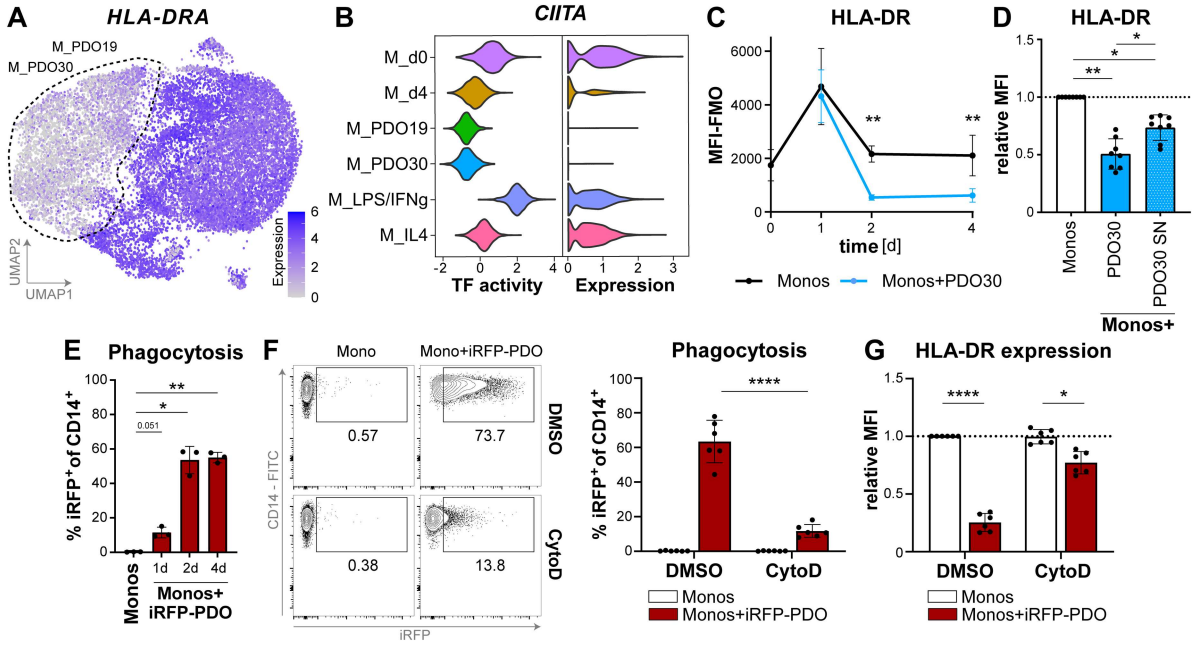

Figure 5. Phagocytosis of PDOs regulates MHC class II expression in monocytes during co-culture. (A) UMAP showing expression of *HLA-DRA* in monocytes of all culture conditions. The encircled area highlights cells derived from PDO co-culture. (B) Inferred CIITA transcription factor (TF) activity based on DoRothEA regulon analysis (left) and *CIITA* expression (right) across monocytes of all culture conditions. (C) Expression of HLA-DR protein on live CD45$^+$ monocytes from monoculture or co-culture with PDO30 over time, as assessed by flow cytometry. Mean ± SD, $N = 5$, Two-Way ANOVA, $^{**}p < 0.01$. (D) Relative expression of HLA-DR on monocytes after 4 days of co-culture with PDO30 or monocytes treated with supernatant (SN) from PDO30 monoculture. The data was normalized to expression of monocyte from monoculture. Mean ± SD, $N = 8$. One-Way ANOVA, $^{*}p < 0.05$, $^{**}p < 0.01$. (E) Phagocytosis by monocytes during co-culture with iRFP-PDO measured by flow cytometry at indicated timepoints. Phagocytosis was identified by the frequency of iRFP$^+$ population of total CD14$^+$ cells. Mean ± SD, $N = 3$, One-Way ANOVA, $^{*}p < 0.05$, $^{**}p < 0.01$. (F) Representative dot plot of monocytes after two days of co-culture with iRFP-PDO in the presence of Cytochalasin D (CytoD) or solvent control (DMSO). Quantification of iRFP$^+$ CD14$^+$ monocytes is displayed on the right. Mean ± SD, $N = 6$, Two-Way ANOVA, $^{****}p < 0.0001$. (G) Normalized expression of HLA-DR on monocytes in (F). The MFI was normalized to the respective monocyte monoculture. Mean ± SD, $N = 3$, One-Way ANOVA, $^{*}p < 0.05$, $^{****}p < 0.0001$.

In summary, phagocytic uptake of PDO cells and debris contributed to the reduction of HLA-DR expression on monocytes and inhibiting this process maintained the monocyte antigen-presentation capability in co-culture.

PDO-exposed monocytes display an impaired response to TLR stimulation

Our co-cultures provide an attractive opportunity to interrogate the functional capabilities of IL1B-programmed monocytes. Given that intratumoral bacteria are a well-known source of inflammatory stimuli in patients with CRC,[35] we stimulated PDO-programmed monocytes with ligands targeting the TLR pathway and analyzed their subsequent production of the pro-inflammatory molecule TNF-α (Figure 6A). PDO30 was selected for this experiment as it lacked TLR1/2/4 expression (Supplemental Table S4).

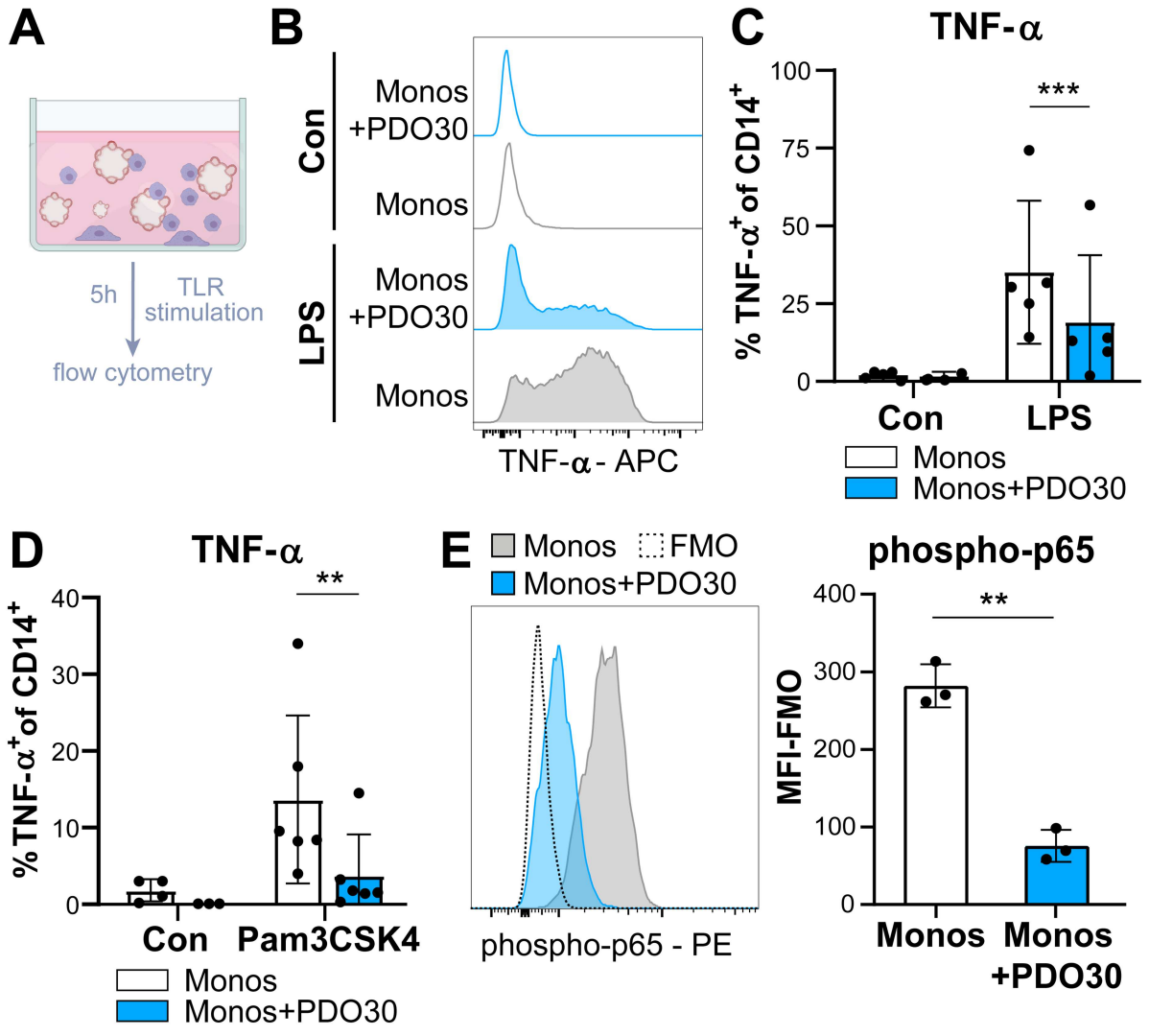

Figure 6. Monocytes in PDO co-culture are less responsive to TLR stimulation. (A) Experimental set-up of TLR stimulation during PDO co-culture. Cells were stimulated for 5 h with LPS or Pam3CSK4, or left untreated (control) in the presence of BrefeldinA prior to harvest. (B,C) Frequency of TNF-α$^+$ monocyte population retrieved from PDO30 co-culture or control monoculture after TLR stimulation with LPS, as quantified by flow cytometry. Representative histograms of live CD14$^+$ monocytes are shown in (B). Mean ± SD, $N = 3–5$, Two-Way ANOVA, $^{**}p < 0.01$. (D) Frequency of TNF-α$^+$ monocytes retrieved from PDO30 co-culture or control monoculture after TLR stimulation with Pam3CSK4, as quantified by flow cytometry. Mean ± SD, $N = 3–6$, Two-Way ANOVA, $^{**}p < 0.01$, $^{***}p < 0.001$. (E) Quantification of phospho-p65 protein in permeabilized CD45$^+$ monocytes after four days of co-culture with PDO30. Representative histogram is shown on the right. Mean ± SD, $N = 3$, paired t-test, $^{**}p < 0.01$.

While monocytes co-cultured with PDO30 produced TNF-α upon LPS stimulation, they did so at lower amounts compared to monocytes from monoculture (Figure 6B and C). Similarly, stimulation with Pam3CSK4, a TLR1/2 agonist, elicited a blunted monocyte response (Figure 6D). To address the underlying mechanism eliciting differential pro-inflammatory cytokine production in co-culture, we examined the NF-κB pathway activity in monocytes by measuring phosphorylation of the p65 subunit, part of the most abundant heterodimer of NF-κB activated by the canonical pathway.[34] Cells co-cultured for four days with PDO30 exhibited reduced levels of phosphorylated p65 protein compared to monocultured monocytes (Figure 6E). This suggested that exposure to PDOs might lead monocytes to transition to a state, reminiscent of the "refractory" phenotype observed upon repeated endotoxin challenge.[36]

Discussion

Organoid technology offers the opportunity to study the spectrum of human CRC biology, maintaining patient-specific features of carcinoma cells in culture over an extended period of time.[37,38] While recapitulating tumor tissue architecture and preserving cellular heterogeneity, PDOs are largely deprived of other cells present in the TME, including monocytes and macrophages.[11] PDO/myeloid cell co-cultures allow the study of myeloid-cancer cell interactions in a 3D setting, while retaining patient-specific tumor characteristics.

Here, we studied eight PDOs derived from individual patients with microsatellite-stable CRC, encompassing heterogeneous mutational backgrounds that reflect the mutational landscape characteristics of CRC.[16] Upon encountering different PDOs *in vitro*, primary monocytes exhibited remarkably similar phenotypic changes beyond the M1/M2 dichotomy,[32,33] independent of patient-specific PDO mutational profiles. scRNA-seq analysis revealed that this phenotype resembled the transcriptomic profile of IL1B monocytes, reported to represent more than 27% of the monocyte/macrophage compartment in CRC patients compared to 7% in healthy colon tissue.[9] IL1B monocytes were found to accumulate to a lesser extent in other cancer entities, where they were predominantly associated with poor patient prognosis.[39] Fate-mapping of monocytes in mouse pancreatic ductal adenocarcinoma (PDAC) showed that IL1B-programmed cells emerged largely from circulating monocytes as the first differentiation state upon migration into the tumor bed.[40,41] Thus, we postulate that PBMC-derived monocytes from healthy buffy coats, a readily available myeloid cell source, can be used to recapitulate features of this early programming of monocytes in cancer. Whether the IL1B-like identity of monocytes exposed to CRC PDOs can be mimicked by PDOs from other malignancies remains to be determined.

Beyond the expression of *IL1B* and related genes of the inflammasome pathway, eicosanoid biosynthesis (*PTGS2*), tissue-repair properties including angiogenesis (*EREG, VEGFA*), and chemotactic factors for neutrophil attraction (*CXCL1, CXCL2*) have been described as core features of IL1B monocytes.[41] In our system, the majority of these previously defined transcripts were differentially expressed except of *PTGS2* and other prostaglandin biosynthesis enzymes, suggesting that PDO-exposed monocytes captured most, but not all, aspects of the IL1B program detected *in situ*.

Our data showed that monocytes secreted various CXCL chemokines after contact with PDOs. PGE_2 and TNF-α were recently described to induce the expression of genes associated with the IL1B phenotype, including CXCLs.[41] The soluble factors driving chemokine secretion in our monocyte/PDO co-cultures remain to be identified. In CRC, myeloid-derived CXCL2/5/7 chemokines may contribute to the establishment of an immunosuppressive TME by recruiting other immune cells. Accordingly, spatial analyzes revealed a close proximity between immunosuppressive neutrophils and inflammasome-activated monocytes in CRC.[2,42] In addition to shaping the immune landscape, myeloid-derived CXCLs have been implicated in chemotherapy resistance. CXCL7 has been shown to promote chemoresistance via CXCR2 signaling in CRC cell lines.[43] Together, these findings implicate myeloid-derived CXCL signaling as a mechanism linking inflammation, pro-tumor function, and drug resistance in cancer.

We further observed that monocytes in co-culture with CRC PDOs displayed reduced antigen presentation capabilities marked by lower expression of MHC class II molecules and co-stimulatory ligand CD86, expanding the characteristics of IL1B monocytes. In contrast to pro-inflammatory signaling networks mediated by soluble factors from cancer organoids, the observed HLA-DR repression on the myeloid cell surface depended on direct contact with PDOs and phagocytosis. In support of a central role

for phagocytosis, a recent study in a murine lung cancer model reported reduced expression of MHC class II molecules and co-stimulatory ligands in myeloid cells extracted from the tumor that contained phagocytosed tumor material.[44] It remains to be determined whether reduced HLA-DR expression on myeloid cells is restricted to IL1B-expressing monocyte states or whether additional monocyte/macrophage states are similarly affected in the tumor context.

In addition to this diminished antigen presentation and co-stimulation capacity, we found further evidence for a potential direct immunosuppressive activity of PDO-exposed monocytes, e.g. the upregulation of ectonucleotidase CD73, leading to the generation of immunosuppressive extracellular adenosine. Additional axes of direct T cell inhibition by immunosuppressive monocyte subsets in CRC have been described, such as the secretion of thrombospondin-1 (THBS1),[45] which we also identified as a DEG in our PDO-exposed monocytes. Thus, the IL1B-associated monocyte state may share functional features with previously described immunosuppressive monocyte subsets. It remains to be tested which axis of T cell modulation—a lack of antigen presentation, co-stimulation, immunosuppressive mediators, or additional pathways—are predominantly utilized by IL1B-associated monocytes within the CRC TME. Notably, their concomitant inflammatory features suggest a dual functional potential, enabling participation in both immunosuppressive and pro-inflammatory immune responses. Elucidating this balance will require further *in vivo* investigation, for example using PDO-derived xenograft models, to more precisely define the functional roles of IL1B-programmed monocytes in CRC.

We describe the expression of transcriptional programs related to further differentiated hypoxia-associated and lipid-binding TAMs in monocytes after encountering PDOs, suggesting that tumor cells prime them at the stage of early infiltration for cancer-supporting fates. Their eventual differentiation "flavor" may depend on nutrient availability and crosstalk with other TME components, since in PDAC spatial analysis demonstrated that lipid-binding TAMs interact with NK/T cells and dendritic cells, whereas hypoxia-associated TAMs were enriched in hypoxic fibroblast- and neutrophil-rich niches.[40] Accordingly, the addition of cancer-associated fibroblasts (CAF) in co-cultures of monocyte-derived macrophages and PDOs promoted the acquisition of a hypoxia-related SPP1$^+$ TAM program, whereas the IL1B program was not amplified by the presence of CAFs.[13] SPP1$^+$ TAMs have gained increasing attention owing to their strong association with poor clinical outcome, and their ability to suppress cytotoxic T cells.[7,8] Accumulation of SPP1$^+$ TAMs correlated with immunosuppression and angiogenesis in a number of cancer entities, although their precise mode of action is subject of ongoing investigation.[46,47] Their developmental origin in CRC remains ambiguous, as both the reprogramming of tissue-resident macrophages and differentiation from circulating monocytes have been proposed.[7] Although our co-culture model does not capture the full trajectory of TAM development from circulating monocytes, it could provide a starting point to dissect whether SPP1$^+$ TAM differentiation is primarily a matter of temporal progression or requires additional cellular components that govern TAM subset specification. Notably, systemic influences on myeloid differentiation in cancer patients, such as tumor-driven emergency myelopoiesis and hematopoietic stem and progenitor cell pre-conditioning, are not captured in our *in vitro* monocyte co-culture model. Given this multi-level regulation of tumor-associated myeloid differentiation, further *in vivo* mouse models or patient-matched PDO–monocyte studies will be required to resolve how local and systemic factors jointly shape TAM differentiation.

Deciphering the contribution of individual states of monocytes and macrophages to tumor-derived chronic inflammation in the TME remains a challenge, owing to their high plasticity and the lack of well-defined markers that unambiguously distinguish TAM states. Our *in vitro* system allowed us to interrogate the functional capacity of PDO-programmed monocytes mimicking the IL1B phenotype. Stimulation of monocytes in PDO co-culture with TLR agonists resulted in the production of pro-inflammatory cytokines, albeit to a lesser extent than in monocytes cultured without PDOs. This reduced cytokine response is reminiscent of the refractory state associated with delayed NF-κB activation, as described in murine macrophages of chronically inflamed advanced tumor models in the early 2000.[48-50] In line with these studies, we observed reduced levels of phosphorylated p65 in monocytes after cancer organoid co-culture. However, we found no evidence for the previously reported mechanism in our scRNA-seq analysis—namely increased *IL10* and *TGFB1* expression, or reduced gene expression of members of the NF-κB or C/EBP family. This highlights the context-specific regulation

of NF-κB activation in TAMs, urging to go beyond transcriptional analysis to delineate the response of individual myeloid subsets. Consistent with this notion, our pathway analysis of PDO-exposed monocytes predicted the involvement of additional pro-inflammatory pathways such as MAPK or STAT signaling, implying that multiple signaling axes may cooperatively shape monocyte phenotype and function in PDO co-culture. Finally, while the transcriptional overlap of PDO-exposed monocytes with patient-derived monocyte states suggests that similar hypo-responsiveness programs may be active in CRC *in vivo*, functional validation of an attenuated inflammatory responsiveness in tumor-infiltrating monocytes remains an area for further investigations.

In conclusion, our monocyte/PDO platform enables the *in vitro* generation of monocyte subsets relevant to CRC patients, providing a means to screen myeloid responses to tumors from individual patients, to dissect the signals driving the acquisition of this phenotype, as well as to test their functional capacities. Ultimately, this modular co-culture system could be utilized to systematically investigate the interactions with additional components of the TME, such as fibroblasts and other immune cells, to advance our understanding of the determinants driving myeloid differentiation in the TME, thereby bridging experimental modeling with clinical heterogeneity, and supporting the development of TAM-targeting therapies for CRC patients.

Disclosure of potential conflicts of interest

L.H. is an employee of EMD Serono Research & Development Institute, Inc., Billerica, MA, USA. The remaining authors declare no competing interests.

Acknowledgments

We would like to acknowledge Dr. Gina Walter-Bausch (The healthcare business of Merck KGaA, Darmstadt, Germany) for collaboration and scientific input, and Alessia Triassi and Anette Funk for the technical support (MI3, Medical Faculty Mannheim, Heidelberg University, Mannheim, Germany). We acknowledge Dr. Carolina de la Torre, Dr. Katharina Mößinger, Angelika Duda, Marina Talamini as well as Carsten Sticht of the Next Generation Sequencing core facility for outstanding support (CFPM, Medical Faculty Mannheim, Heidelberg University, Mannheim, Germany). We acknowledge support by the state of Baden-Württemberg through bwHPC and the German Research Foundation (DFG) through grant INST 35/1597-1 FUGG. We also gratefully acknowledge the data storage service SDS@hd supported by the Ministry of Science, Research and the Arts Baden-Württemberg (MWK) and the DFG through grant INST 35/1503-1 FUGG. We thank Stefanie Uhlig (FlowCore Mannheim, CFPM, Medical Faculty Mannheim, Heidelberg University, Mannheim, Germany) for her excellent technical support. We further thank the group of Prof. Dr. Karen Bieback from the Institute of Transfusion Medicine and Immunology, especially Isabell Moskal and Susanne Elvers-Hornung, for the opportunity and their technical support to use the IncuCyte SX5TM (Medical Faculty Mannheim, Heidelberg University, Mannheim, Germany). We also thank the German Red Cross Blood Donor Service Baden-Württemberg—Hessen, Institute Mannheim, for providing buffy coats.

All authors contributed to and approved the article submission. B.B. designed the project, performed and analyzed the experiments, conducted bioinformatical analysis, interpreted the data, wrote and revised the manuscript. S.H. and A.v K. performed experiments and helped with PDO handling and set-up. I.A.S. supported the confocal live-cell imaging experiment. K.B. generated the iRFP-PDO line and critically reviewed the manuscript. V.A. supported the bioinformatic analysis. E.B., J.B., M.E., and M.B. generated and provided PDOs, supported the methodology and acquired funding. L.H. helped with the project design and provided scientific input. V.U. critically reviewed the manuscript. A.C. acquired funding, designed and supervised the project, helped with writing and revising the manuscript.

Funding

The work was supported by the German Research Foundation: SFB1366 (Project number 394046768-SFB 1366; C02 to AC), SPP 1937 (CE 140/2-2 827 to A.C.), TRR179 (TP07 to A.C.), SFB-TRR156 (B10N to A.C.), SFB 1709/1 – 533056198 (project B06 to A.C.) and RTG2727–45549683 (B1.2 to A.C. and B1.3 to E.B. and M.E.) and ExU 829 6.1.11 (to A.C.) and by the German Cancer Aid translational oncology program "NK fit against AML" (74114180) (to A.C.), the Merck Heidelberg Innovation Call and the healthcare business of Merck KGaA, Darmstadt, Germany (CrossRef Funder ID: 10.13039/100009945).

Author contributions

CRediT: **Bianca M. Balzasch:** Conceptualization, Data curation, Formal analysis, Investigation, Methodology, Project administration, Software, Validation, Visualization, Writing – original draft; **Andreas von Kries:** Methodology; **Saskia Hüll:** Investigation; **Indra A. Shaltiel:** Investigation; **Kim E. Boonekamp:** Methodology, Resources, Writing – review & editing; **Volker Ast:** Software; **Elke Burgermeister:** Funding acquisition, Methodology, Resources; **Johannes Betge:** Methodology, Resources; **Matthias Ebert:** Funding acquisition, Methodology, Resources; **Michael Boutros:** Funding acquisition, Methodology, Resources; **Laura Helming:** Writing – review & editing; **Viktor Umansky:** Writing – review & editing; **Adelheid Cerwenka:** Conceptualization, Funding acquisition, Project administration, Supervision, Writing – review & editing.

ORCID

Bianca M. Balzasch 0009-0006-0038-4413
Andreas von Kries 0000-0002-7425-2329
Indra A. Shaltiel 0000-0002-5673-6741
Kim E. Boonekamp 0000-0002-9968-5382
Elke Burgermeister 0000-0002-4969-5697
Johannes Betge 0000-0001-9549-1866
Laura Helming 0009-0005-6268-2101
Viktor Umansky 0000-0003-0259-1839

Data availability statement

Raw data were generated at UMM NGS core facility of the University Heidelberg. Derived data supporting the findings of this study are available from the corresponding author A.C. upon reasonable request. Single-cell and bulk RNA sequencing data generated in this study are deposited in NCBI's Gene Expression Omnibus (GEO) and are accessible through accession number GSE308582 and GSE308548, respectively.

Ethics approval statement

The Ethic Commission II of the Medical Faculty Mannheim, Heidelberg University (Reference no. 2014–633N-MA and 2016–607N-MA) approved the collection of colorectal cancer tissue biopsies, generation of cancer organoids, and subsequent experiments.

Primary human monocytes were isolated from buffy coats of healthy donors obtained from the blood bank of the DRK-blood donation service Baden-Württemberg-Hessen (Mannheim, Germany). The Ethic Commission II of the Medical Faculty Mannheim, Heidelberg University granted ethical approval 87/04.

Patient consent statement

All CRC patients and blood donors gave written informed consent.

References

1. Guinney J, Dienstmann R, Wang X, de Reyniès A, Schlicker A, Soneson C, Marisa L, Roepman P, Nyamundanda G, Angelino P, et al. The consensus molecular subtypes of colorectal cancer. Nat Med. 2015;21:1350–1356. doi: 10.1038/nm.3967.
2. Pelka K, Hofree M, Chen JH, Sarkizova S, Pirl JD, Jorgji V, Bejnood A, Dionne D, Ge WH, Xu KH, et al. Spatially organized multicellular immune hubs in human colorectal cancer. Cell. 2021;184:4734–4752.e20. doi: 10.1016/j.cell.2021.08.003.
3. Chu X, Li X, Zhang Y, Dang, G, Miao, Y, Xu, W, Wang, J, Cheng, S. Integrative single-cell analysis of human colorectal cancer reveals patient stratification with distinct immune evasion mechanisms. Nat Cancer. 2024;5:1409–1426. doi: 10.1038/s43018-024-00807-z.
4. Zhang Q, Liu L, Gong C, Shi H, Zeng Y, Wang X, Zhao Y, Wei Y, Hoque MO. Prognostic significance of tumor-associated macrophages in solid tumor: a meta-analysis of the literature. PLoS One. 2012;7:e50946. doi: 10.1371/journal.pone.0050946.
5. Park MD, Silvin A, Ginhoux F, Merad M. Macrophages in health and disease. Cell. 2022;185:4259–4279. doi: 10.1016/j.cell.2022.10.007.

6. Liu Z, Gu Y, Chakarov S, Bleriot C, Kwok I, Chen X, Shin A, Huang W, Dress RJ, Dutertre C, et al. Fate mapping via Ms4a3-Expression history traces monocyte-derived cells. Cell. 2019;178:1509–1525.e19. doi: 10.1016/j.cell.2019.08.009.
7. Zhang L, Li Z, Skrzypczynska KM, Fang Q, O'Brien SA, He Y, Wang L, Kim A, Gao R, Orf J, et al. Single-cell analyses inform mechanisms of myeloid-targeted therapies in colon cancer. Cell. 2020;181:442–459.e29. doi: 10.1016/j.cell.2020.03.048.
8. Lee H-O, Hong Y, Etlioglu HE, Cho YB, Pomella V, Van den Bosch B, Vanhecke J, Verbandt S, Min J, Kim N, et al. Lineage-dependent gene expression programs influence the immune landscape of colorectal cancer. Nat Genet. 2020;52:594–603. doi: 10.1038/s41588-020-0636-z.
9. Mulder K, Patel AA, Kong WT, Piot C, Halitzki E, Dunsmore G, Khalilnezhad S, Irac SE, Dubuisson A, Chevrier M, et al. Cross-tissue single-cell landscape of human monocytes and macrophages in health and disease. Immunity. 2021;54:1883–1900.e5. doi: 10.1016/j.immuni.2021.07.007.
10. Monnier M, Paolini L, Vinatier E, Mantovani A, Delneste Y, Jeannin P. Antitumor strategies targeting macrophages: the importance of considering the differences in differentiation/polarization processes between human and mouse macrophages. J Immunother Cancer. 2022;10:e005560. doi: 10.1136/JITC-2022-005560.
11. Tuveson D, Clevers H. Cancer modeling meets human organoid technology. Science. 2019;364(1979):952–955. doi: 10.1126/science.aaw6985.
12. Wang J, Tao X, Zhu J, Dai Z, Du Y, Xie Y, Chu X, Fu G, Lei Z. Tumor organoid-immune co-culture models: exploring a new perspective of tumor immunity. Cell Death Discov. 2025;11:195. doi: 10.1038/s41420-025-02407-x.
13. Li N, Zhu Q, Tian Y, Ahn KJ, Wang X, Cramer Z, Jou J, Folkert IW, Yu P, Adams-Tzivelekidis S, et al. Mapping and modeling human colorectal carcinoma interactions with the tumor microenvironment. Nat Commun. 2023;14:7915. doi: 10.1038/s41467-023-43746-6.
14. Kabiljo J, Theophil A, Homola J, Renner AF, Stürzenbecher N, Ammon D, Zirnbauer R, Stang S, Tran L, Laengle J, et al. Cancer-associated fibroblasts shape early myeloid cell response to chemotherapy-induced immunogenic signals in next generation tumor organoid cultures. J Immunother Cancer. 2024;12:e009494. doi: 10.1136/jitc-2024-009494.
15. Fang H, Huang Y, Luo Y, Tang J, Yu M, Zhang Y, Zhong M. SIRT1 induces the accumulation of TAMs at colorectal cancer tumor sites via the CXCR4/CXCL12 axis. Cell Immunol. 2022;371:104458. doi: 10.1016/j.cellimm.2021.104458.
16. Betge J, Rindtorff N, Sauer J, Rauscher B, Dingert C, Gaitantzi H, Herweck F, Srour-Mhanna K, Miersch T, Valentini E, et al. The drug-induced phenotypic landscape of colorectal cancer organoids. Nat Commun. 2022;13(1):1–15. doi: 10.1038/s41467-022-30722-9.
17. popscle. https://github.com/statgen/popscle
18. Hao Y, Stuart T, Kowalski MH, Choudhary S, Hoffman P, Hartman A, Srivastava A, Molla G, Madad S, Fernandez-Granda C, et al. Dictionary learning for integrative, multimodal and scalable single-cell analysis. Nat Biotechnol. 2024;42:293–304. doi: 10.1038/s41587-023-01767-y.
19. Korsunsky I, Millard N, Fan J, Slowikowski K, Zhang F, Wei K, Baglaenko Y, Brenner M, Loh P, Raychaudhuri S. Fast, sensitive and accurate integration of single-cell data with harmony. Nat Methods. 2019;16:1289–1296. doi: 10.1038/s41592-019-0619-0.
20. Finak G, McDavid A, Yajima M, Deng J, Gersuk V, Shalek AK, Slichter CK, Miller HW, McElrath MJ, Prlic M, et al. MAST: a flexible statistical framework for assessing transcriptional changes and characterizing heterogeneity in single-cell RNA sequencing data. Genome Biol. 2015;16:278. doi: 10.1186/s13059-015-0844-5.
21. Gu Z. Complex heatmap visualization. iMeta. 2022;1:e43. doi: 10.1002/imt2.43.
22. Wu T, Hu E, Xu S, Chen M, Guo P, Dai Z, Feng T, Zhou L, Tang W, Zhan L, et al. clusterProfiler 4.0: a universal enrichment tool for interpreting omics data. Innovation. 2021;2:100141. doi: 10.1016/j.xinn.2021.100141.
23. Andreatta M, Carmona SJ. UCell: robust and scalable single-cell gene signature scoring. Comput Struct Biotechnol J. 2021;19:3796–3798. doi: 10.1016/j.csbj.2021.06.043.
24. Schubert M, Klinger B, Klünemann M, Sieber, A, Uhlitz, F, Sauer, S, Garnett, MJ, Blüthgen, N, Saez-Rodriguez, J. Perturbation-response genes reveal signaling footprints in cancer gene expression. Nat Commun. 2018;9:20. doi: 10.1038/s41467-017-02391-6.
25. Badia-i-Mompel P, Vélez Santiago J, Braunger J, Geiss, C, Dimitrov, D, Müller-Dott, S, Taus, P, Dugourd, A, Holland, CH, Ramirez Flores, RO, et al. decoupleR: ensemble of computational methods to infer biological activities from omics data. Bioinformatics Advances. 2022;2. doi: 10.1093/bioadv/vbac016.
26. Groth C, Maric J, Garcés Lázaro I, Hofman, T, Zhang, Z, Ni, Y, Keller, F, Seufert, I, Hofmann, M, Neumann-Haefelin, C, et al. Hepatitis D infection induces IFN-ß-mediated NK cell activation and TRAIL-dependent cytotoxicity. Front Immunol. 2023;14. doi: 10.3389/fimmu.2023.1287367.
27. Recaldin T, Steinacher L, Gjeta B, Harter MF, Adam L, Kromer K, Mendes MP, Bellavista M, Nikolaev M, Lazzaroni G, et al. Human organoids with an autologous tissue-resident immune compartment. Nature. 2024;2024:1–9. doi: 10.1038/s41586-024-07791-5.
28. Shaw TN, Houston SA, Wemyss K, Bridgeman, HM, Barbera, TA, Zangerle-Murray, T, Strangward, P, Ridley, AJ, Wang, P, Tamoutounour, S, et al. Tissue-resident macrophages in the intestine are long lived and defined by Tim-4 and CD4 expression. J Exp Med. 2018;215:1507–1518. doi: 10.1084/jem.20180019.

29. Li J, Wang L, Chen X, Ping Y, Huang L, Yue D, Zhang Z, Yang L, Zhao X, Dong W, et al. CD39/CD73 upregulation on myeloid-derived suppressor cells via TGF-ß-mTOR-HIF-1 signaling in patients with non-small cell lung cancer. Oncoimmunology. 2017;6. doi: 10.1080/2162402X.2017.1320011.
30. Jung K, Heishi T, Incio J, Huang Y, Beech EY, Pinter M, Ho WW, Kawaguchi K, Rahbari NN, Chung E,et al. Targeting CXCR4-dependent immunosuppressive Ly6Clow monocytes improves antiangiogenic therapy in colorectal cancer. Proc Natl Acad Sci. 2017;114:10455–10460. doi: 10.1073/pnas.1710754114.
31. Murray PJ. Macrophage polarization. Annu Rev Physiol. 2017;79:541–566. doi: 10.1146/annurev-physiol-022516-034339.
32. Martinez FO, Gordon S, Locati M, Mantovani A. Transcriptional profiling of the human monocyte-to-macrophage differentiation and polarization: new molecules and patterns of gene expression. J Immunol. 2006;177:7303–7311. doi: JIMMUNOL.177.10.7303" type="start">10.4049/JIMMUNOL.177.10.7303.
33. Azizi E, Carr AJ, Plitas G, Cornish AE, Konopacki C, Prabhakaran S, Nainys J, Wu K, Kiseliovas V, Setty M, et al. Single-cell map of diverse immune phenotypes in the breast tumor microenvironment. Cell. 2018;174:1293–1308.e36. doi: 10.1016/j.cell.2018.05.060.
34. Liu T, Zhang L, Joo D, Sun S. NF-κB signaling in inflammation. Signal Transduct Target Ther. 2017;2(1):1–9. doi: 10.1038/sigtrans.2017.23.
35. Sepich-Poore GD, Zitvogel L, Straussman R, Hasty J, Wargo JA, Knight R. The microbiome and human cancer. Science. 2021;371:1979. doi: 10.1126/science.abc4552.
36. Biswas SK, Lopez-Collazo E. Endotoxin tolerance: new mechanisms, molecules and clinical significance. Trends Immunol. 2009;30:475–487. doi: 10.1016/j.it.2009.07.009.
37. Pauli C, Hopkins BD, Prandi D, Shaw R, Fedrizzi T, Sboner A, Sailer V, Augello M, Puca L, Rosati R, et al. Personalized in vitro and in vivo cancer models to guide precision Medicine. Cancer Discov. 2017;7:462–477. doi: 10.1158/2159-8290.CD-16-1154.
38. Schütte M, Risch T, Abdavi-Azar N, Boehnke K, Schumacher D, Keil M, Yildiriman R, Jandrasits C, Borodina T, Amstislavskiy V, et al. Molecular dissection of colorectal cancer in pre-clinical models identifies biomarkers predicting sensitivity to EGFR inhibitors. Nat Commun. 2017;8:14262. doi: 10.1038/ncomms14262.
39. Caronni N, La Terza F, Frosio L, Ostuni R. IL-1ß+ macrophages and the control of pathogenic inflammation in cancer. Trends Immunol. 2025;46:403–415. doi: 10.1016/j.it.2025.03.001.
40. Dunsmore G, Guo W, Li Z, Bejarano DA, Pai R, Yang K, Kwok I, Tan L, Ng M, De La Calle Fabregat C, et al. Timing and location dictate monocyte fate and their transition to tumor-associated macrophages. Sci Immunol. 2024;9. doi: 10.1126/sciimmunol.adk3981.
41. Caronni N, La Terza F, Vittoria FM, Barbiera G, Mezzanzanica L, Cuzzola V, Barresi S, Pellegatta M, Canevazzi P, Dunsmore G, et al. IL-1ß+ macrophages fuel pathogenic inflammation in pancreatic cancer. Nature. 2023;623:415–422. doi: 10.1038/s41586-023-06685-2.
42. Matusiak M, Hickey JW, van IJzendoorn DGP, Lu G, Kidzinski L, Zhu S, Colburg DR, Luca B, Phillips DJ, Brubaker SW, et al. Spatially segregated macrophage populations predict distinct outcomes in colon cancer. Cancer Discov. 2024;14:1418–1439. doi: 10.1158/2159-8290.CD-23-1300.
43. Liu S, Gong H, Li P, Hu J, Xu R, Cai J, Wang S, Ma H, Mi X, Zhou Q, et al. Chemotherapy-induced macrophage CXCL7 expression drives tumor chemoresistance via the STAT1/PHGDH-serine metabolism axis and SAM paracrine feedback to M2 polarization. Cell Death Dis. 2025;16:379. doi: 10.1038/s41419-025-07712-y.
44. Park MD, Reyes-Torres I, LeBerichel J, Hamon P, LaMarche NM, Hegde S, Belabed M, Troncoso L, Grout JA, Magen A, et al. TREM2 macrophages drive NK cell paucity and dysfunction in lung cancer. Nat Immunol. 2023;24:792–801. doi: 10.1038/s41590-023-01475-4.
45. Omatsu M, Nakanishi Y, Iwane K, Aoyama N, Duran A, Muta Y, Martinez-Ordoñez A, Han Q, Agatsuma N, Mizukoshi K, et al. THBS1-producing tumor-infiltrating monocyte-like cells contribute to immunosuppression and metastasis in colorectal cancer. Nat Commun. 2023;14:5534. doi: 10.1038/s41467-023-41095-y.
46. Trehan R, Huang P, Zhu XB, Wang X, Soliman M, Strepay D, Nur A, Kedei N, Arhin M, Ghabra S, et al. SPP1+ macrophages cause exhaustion of tumor-specific T cells in liver metastases. Nat Commun. 2025;16:4242. doi: 10.1038/s41467-025-59529-0.
47. Bill R, Wirapati P, Messemaker M, Roh W, Zitti B, Duval F, Kiss M, Park JC, Saal TM, Hoelzl J, et al. CXCL9:SPP1 macrophage polarity identifies a network of cellular programs that control human cancers. Science. 2023;381(1979):515–524. doi: 10.1126/science.ade2292.
48. Torroella-Kouri M, Ma X, Perry G, Ivanova M, Cejas PJ, Owen JL, Iragavarapu-Charyulu V, Lopez DM. Diminished expression of transcription factors nuclear factor κB and CCAAT/Enhancer binding protein underlies a novel tumor evasion mechanism affecting macrophages of mammary Tumor–Bearing mice. Cancer Res. 2005;65:10578–10584. doi: 10.1158/0008-5472.CAN-05-0365.
49. Sica A, Saccani A, Bottazzi B, Polentarutti N, Vecchi A, Van Damme J, Mantovani A. Autocrine production of IL-10 mediates defective IL-12 production and NF-kappa B activation in tumor-associated macrophages. J Immunol. 2000;164:762–767. doi: 10.4049/jimmunol.164.2.762.
50. Biswas SK. A distinct and unique transcriptional program expressed by tumor-associated macrophages (defective NF- B and enhanced IRF-3/STAT1 activation). Blood. 2006;107:2112–2122. doi: 10.1182/blood-2005-01-0428.